

Minimal models and transport properties of unconventional p -wave magnets

Bjørnulf Brekke,^{1,*} Pavlo Sukhachov,^{1,*} Hans Gløckner Gilil,¹ Arne Brataas,¹ and Jacob Linder¹

¹*Center for Quantum Spintronics, Department of Physics, Norwegian University of Science and Technology, NO-7491 Trondheim, Norway*

(Dated: May 23, 2024)

New unconventional compensated magnets have been discovered in the wake of altermagnets. We introduce a minimal tight-binding model with a spin-split p -wave band structure, clarifying the relation between unconventional p -wave magnets and helimagnets. Motivated by the tight-binding model, we construct an effective model suitable for analytical calculations. We evaluate the tunneling conductance in junctions with p -wave magnets, revealing a large magnetoresistance despite the absence of a net magnetization. The bulk transport properties reveal anisotropic spin conductivity beyond linear response. These results show that unconventional p -wave magnets offer several useful functionalities for spintronics devices.

Introduction.— Recently, the new class of magnetic materials with collinear magnetic order dubbed altermagnets has attracted significant attention [1–8]. Like conventional antiferromagnets, altermagnets are compensated and do not produce magnetic stray fields. Yet, they feature fully spin-polarized itinerant electrons with a large nonrelativistic spin splitting, rendering the spin-degree of freedom accessible for spin transport [9–13], spin-caloritronics [14–18] and superconductivity [19–33]. Many material candidates, such as Ru₂O [34], MnF₂, MnTe, and CrSb have been suggested, see also Ref. [2]. Experimental verification of spin-split electron bands quickly followed their discovery [35–40].

Altermagnets are classified by the spin space groups, which describe the symmetry properties of magnets with negligible coupling between the crystal lattice and spin spaces [41–44]. The spin space groups showcase magnetic properties that do not rely on the relativistic spin-orbit coupling (SOC) between itinerant electrons and localized magnetic moments. In addition to collinear magnets, the spin space groups can be used to classify non-collinear and non-coplanar magnets [45, 46].

In contrast to collinear magnets, non-collinear and non-coplanar magnets can host itinerant spin-split electron bands with an unconventional p -wave symmetry induced by an isotropic sd-spin interaction [47, 48]. The presence of a composite $\mathcal{T}\tau$ symmetry protects the p -wave spin-polarization in non-centrosymmetric and non-collinear magnets [48]; here, \mathcal{T} is the time-reversal operator and τ denotes a translation, typically by half a unit cell. This symmetry makes p -wave magnets distinct from helimagnets, where the p -wave spin-polarization can also be observed [47, 49, 50]. While p -wave magnets were classified and material candidates, such as Mn₃GaN and CeNiAsO, were proposed in Ref. [48], the potential spintronics applications and even minimal models of p -wave magnets remain unexplored.

In this Letter, we fill this knowledge gap and propose a minimal tight-binding model of an unconventional p -wave magnet. Based on this model, we formulate an effective low-energy Hamiltonian suitable for analytical calculations.

As an application of the model and a manifestation of the p -wave nature of unconventional magnets, we predict a large tunneling magnetoresistance (TMR) in junctions of p -wave magnets with the qualitatively different dependence on the relative orientation of the spin-spin Fermi surfaces: unlike d -wave altermagnets, the antiparallel configuration of spins needed for TMR is achieved by rotating the p -wave magnet by π rather than $\pi/2$. Finally, we show that while p -wave magnets feature an equilibrium spin current, applying an electric field also produces a non-equilibrium transport spin current to the second order in the applied field. The p -wave magnet also filters injected spin currents from a different material. The TMR and spin currents provide effective means to detect and utilize p -wave magnets in spintronics.

Symmetry groups and minimal models for p -wave antiferromagnets.— Electron spin splitting can arise in magnets with broken \mathcal{PT} symmetry, where \mathcal{P} is the inversion operator. Altermagnets have even parity spin-split electron bands consistent with rotational symmetry. This rotational symmetry prohibits net magnetization and ensures the altermagnet is fully compensated; it is a defining property of altermagnets. In contrast, the absence of magnetization in p -wave magnets is enforced by a composite $\mathcal{T}\tau$ symmetry. Here, we consider spin-polarized electron bands with a p -wave character mediated by spin-spin interactions, protected by this $\mathcal{T}\tau$ symmetry. We take this as the definition of unconventional p -wave magnets [48].

As an example of a coplanar p -wave magnet, we propose the minimal lattice model shown in Fig. 1a. The lattice is centrosymmetric. However, the magnetic ordering breaks both \mathcal{P} and \mathcal{PT} symmetries. Since the spin rotates by $\pi/2$ between each lattice site, the proposed model belongs to the class of helimagnets (cycloidal magnets). However, the $\mathcal{T}\tau$ symmetry, crucial for unconventional p -wave magnets, is not a general property of helimagnets. For example, helimagnets, where the spin rotates by $2\pi/(2n+1)$ with $n \in \mathbb{Z}$, have no $\mathcal{T}\tau$ symmetry and are not guaranteed to have a p -wave spin polarization for the itinerant electrons. We note that a p -wave polar-

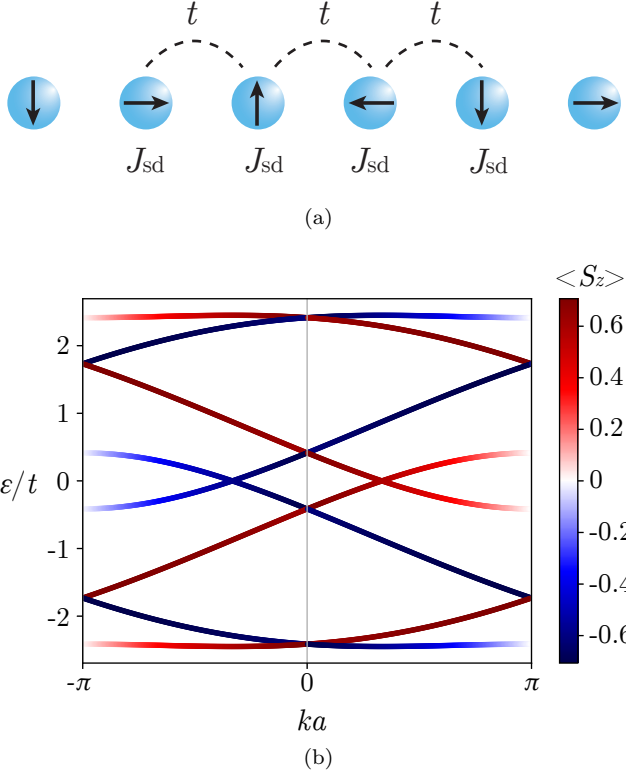


FIG. 1. (a) A minimal magnetic lattice for p -wave magnetism. The nearest neighbor sites are coupled by hopping t , and the itinerant electrons interact with the localized spins by an sd interaction J_{sd} . (b) The electron band structure with spin polarization $\langle S_z \rangle$ of the bands in units of $\hbar/2$ shown in red and blue. The bands are plotted for parameters $J/t = 1$ and $\mu/t = 0$ in Eq. (1).

ization can be protected by other accidental symmetries. These symmetries, however, tend to be less robust than the $\mathcal{T}\tau$ symmetry.

The minimal p -wave magnetic lattice in Fig. 1a is described by the following tight-binding model:

$$H_e = -t \sum_{\langle i,j \rangle, \sigma} c_{i,\sigma}^\dagger c_{j,\sigma} - \mu \sum_{i,\sigma} c_{i,\sigma}^\dagger c_{i,\sigma} - J_{\text{sd}} \sum_{i,\sigma,\sigma'} \mathbf{S}_i \cdot c_{i,\sigma}^\dagger \boldsymbol{\sigma} \sigma \sigma' c_{i,\sigma'}, \quad (1)$$

where $c_{i,\sigma}^{(\dagger)}$ is the electron (creation) annihilation operator for an electron with spin σ at site i . The parameter t corresponds to hopping between nearest neighbors $\langle i,j \rangle$, μ is the chemical potential, and J_{sd} is the isotropic sd-coupling between a localized spin and itinerant electrons. The tight-binding Hamiltonian features p -wave spin-polarized bands, as shown in Fig. 1b. The spin polarization of the electron bands is collinear and perpendicular to all localized spins, such that $\langle S_x \rangle = \langle S_y \rangle = 0$.

Phenomenological model for itinerant electrons in p -wave magnets.— Motivated by the minimal lattice model in Fig. 1a, we propose an effective model for itinerant

electrons in a p -wave magnet

$$H_{\text{eff}} = (-2t [\cos(k_x a) + \cos(k_y a)] - \mu) \sigma_0 \otimes \tau_0 + [\alpha_x \sin(k_x a) + \alpha_y \sin(k_y a)] \sigma_{z'} \otimes \tau_0 + J_{\text{sd}} \sigma_{x'} \otimes \tau_z. \quad (2)$$

Here, σ_i and τ_i are Pauli matrices acting on the spin space and the degree of freedom spanned by the two sectors depicted as red and gray ovals in Fig. 2. The spin coordinates are primed to emphasize that they are decoupled from the crystal coordinates. Here, t denotes the intra-sectoral hopping shown in Fig. 2, the net sd-coupling within a sector is given by J_{sd} , and a is the length of the primitive lattice vectors. Within the effective model, each site hosts two localized spins. Consequently, the model becomes effectively collinear by a unitary spin-space rotation. For this reason, we add spin-dependent hopping with strengths α_x and α_y to recover the non-collinear magnetic nature of the model. The subscripts x and y refer to the crystal directions and follow from a natural two-dimensional generalization of the model. We neglect inter-sectoral hopping for convenience since it does not affect the defining properties of the p -wave magnet. Consequently, the effective model is a 4×4 Hamiltonian block-diagonal in the sectoral degree of freedom.

The four electron bands are two-fold degenerate with energies given by

$$\varepsilon_{\pm} = -2t [\cos(k_x a) + \cos(k_y a)] - \mu \pm \sqrt{J_{\text{sd}}^2 + [\alpha_x \sin(k_x a) + \alpha_y \sin(k_y a)]^2}, \quad (3)$$

where the band splitting is determined by J_{sd} . Each of the degenerate bands is spin-polarized, as exemplified in Fig. 2b. The spin polarization of these two doubly degenerate bands along the crystal k_x -axis is given by

$$\langle S_z \rangle = \pm \frac{2\alpha_x \sin(k_x a)}{\sqrt{J_{\text{sd}}^2 + [\alpha_x \sin(k_x a)]^2}}, \quad (4)$$

in units of $\hbar/2$ whereas the spin polarizations $\langle S_x \rangle$ and $\langle S_y \rangle$ cancel between the degenerate copies.

While the model (3) is topologically trivial, it can be extended to include nontrivial topology. For example, by modulating the effective sd-coupling as $J_{\text{sd}} \rightarrow J_{\text{sd}} \cos(k_x a)$ in Eq. (2), we obtain nonzero winding numbers in each of the sectors [51].

In contrast to altermagnets without spin-orbit coupling, unconventional p -wave magnets feature only partial spin-polarization. This is an integral property of non-collinear magnets. Notably, a strong sd-coupling J_{sd} induces a large spin-splitting but reduces the spin-polarization of the bands, making J_{sd} a trade-off quantity for the potential spintronics properties of unconventional p -wave magnets.

Tunneling magnetoresistance.— As a potential experimental probe of p -wave magnets, we suggest the TMR.

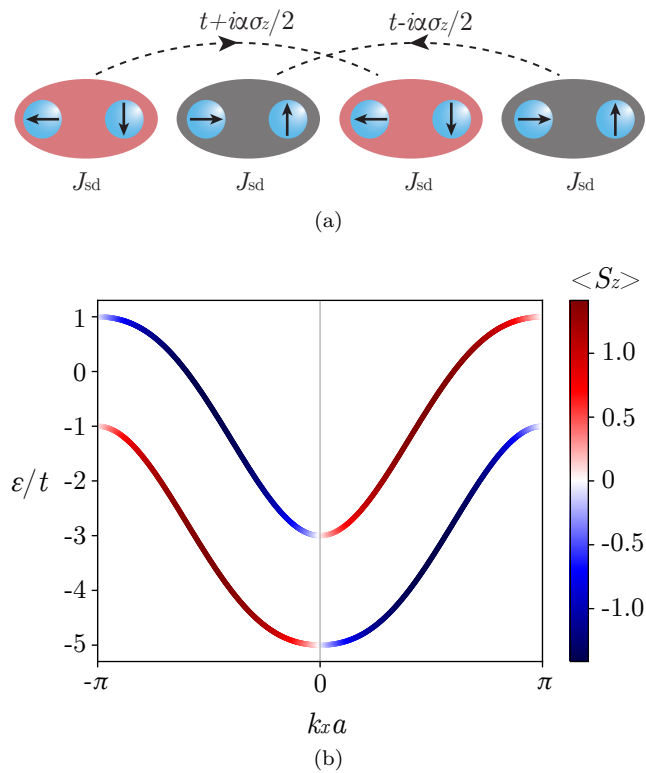


FIG. 2. (a) A lattice model consistent with the effective model in Eq. (2). The model has two sectoral degrees of freedom, as shown in red and grey. (b) The resulting electron bands with spin polarization $\langle S_z \rangle$ in units of $\hbar/2$. The bands are calculated via Eq. (3) with parameters $J_{sd}/t = \alpha/t = 1$ and $\mu/t = 0$.

We calculate the TMR in two model setups involving 2D p -wave magnets: (i) a bilayer and (ii) a planar interface, see Fig. 3a. To make an analytical advance, we consider a low-energy expansion of the Hamiltonian (2):

$$H_\eta(\mathbf{k}) = \left(\frac{k^2}{2m} - \mu \right) \sigma_0 + (\boldsymbol{\alpha}' \cdot \mathbf{k}) \sigma_z + \eta J_{sd} \sigma_x, \quad (5)$$

where $k = \sqrt{k_x^2 + k_y^2}$, $m = 1/(2ta^2)$ is the effective mass, $\boldsymbol{\alpha}' = a\boldsymbol{\alpha}$, and $\eta = \pm$ corresponds to the sectoral degree of freedom.

The TMR is defined as [52]

$$\text{TMR} = \frac{G(\theta_\alpha) - G(\theta_\alpha + \pi)}{G(\theta_\alpha + \pi)}, \quad (6)$$

where $G(\theta_\alpha)$ is the differential conductance between the p -wave magnets calculated at vanishing bias as a function of the relative angle θ_α between the splitting vectors $\boldsymbol{\alpha}_{1,2}$ in the magnets [53]. To calculate the differential conductance, we use the standard tunneling Hamiltonian approach; see Supplemental Material [51] for details of the calculations.

The TMR in the bilayer and the planar junction are shown in Figs. 3b and 3c, respectively. Both junctions al-

low for a sizable TMR that originates from the mismatch of the spin polarizations in the magnets. The p -wave symmetry of the magnets is evident from the periodicity of the TMR. Unlike d -wave magnets (altermagnets) studied in Refs. [9, 12], the maximal TMR is achieved when the magnets are rotated by π rather than $\pi/2$. While both the bilayer and the planar junction offer comparable TMR, the TMR has a larger magnitude and is less sensitive to the mismatch of the Fermi surfaces in the planar junction, cf. Figs. 3b and 3c.

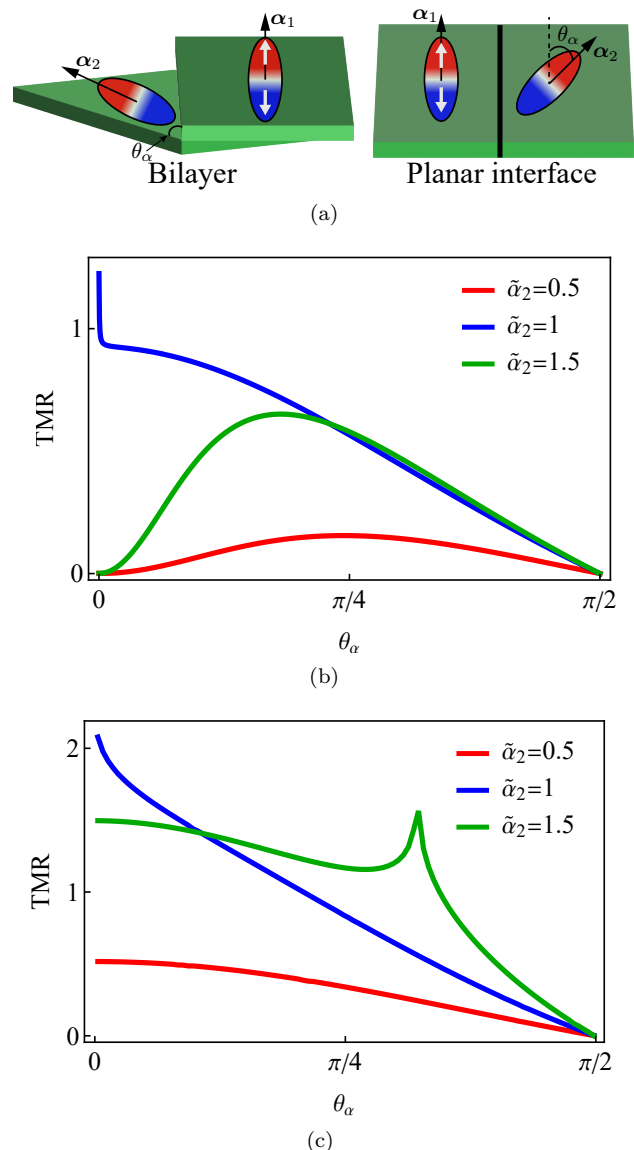


FIG. 3. (a) Model setups of the bilayer and the planar junction of p -wave magnets. (b) TMR as a function of the relative angle θ_α between the spin-splitting vectors $\boldsymbol{\alpha}_1$ and $\boldsymbol{\alpha}_2$ in two layers of the bilayer. (c) The same as (b) in a planar junction, where we fix $\boldsymbol{\alpha}_1$ to be parallel to the interface. The conductance is calculated in the linear response regime, and the tilde denotes the dimensionless parameters $\tilde{J} = J_{sd}/\mu$ and $\tilde{\boldsymbol{\alpha}} = 2m\boldsymbol{\alpha}'/k_F$ with $k_F = \sqrt{2m\mu}$ being the Fermi wave vector. We use $\tilde{J}_1 = \tilde{J}_2 = \tilde{\alpha}_1 = 1$.

Spin conductivity.— As their altermagnetic cousins, p -wave magnets offer a viable route to generate spin currents. For inhomogeneous magnetic textures such as the present system, a spin current exists in equilibrium without any applied bias [54]. This can be intuitively understood based on the Fermi surface of p -wave magnets where carriers with opposite momentum have opposite spin, thus creating a net spin flow along the spin-splitting vector α . Such an exchange spin current should be distinguished from a transport (non-equilibrium) spin current that can be induced by an external bias [55]. By using the semiclassical approach with the collision integral in the relaxation-time approximation, we calculate the first- and second-order response to an electric field in p -wave magnets; see the Supplemental Material [51] for details. For simplicity, we consider the limit of small Fermi energy $|\mu| < |J_{sd}|$ where only the lowest-energy bands, see Fig. 2b, contribute to electric and spin transport; this allows us to neglect inter-band effects.

In the linear-response regime, we find an anisotropic electric conductivity tensor with a vanishing spin conductivity. The anisotropy of the former is the manifestation of the shape of the Fermi surface: electrons moving along α have lower velocity.

The spin current is obtained in the second-order response, $J_i^{(\sigma)} = \chi_{ijl}^{(\sigma)} E_j E_l$. Since the effective model is $\mathcal{T}\tau$ symmetric, the second-order electric current response vanishes. The symmetry of the Fermi surface in the direction perpendicular to α permits only $\chi_{\parallel\parallel\parallel}^{(\sigma)}$, $\chi_{\parallel\perp\perp}^{(\sigma)}$, and $\chi_{\perp\perp\parallel}^{(\sigma)} = \chi_{\perp\parallel\perp}^{(\sigma)}$.

We show the corresponding response coefficients in Fig. 4 as functions of the spin-splitting parameter $\tilde{\alpha}$. Only $\chi_{\parallel\parallel\parallel}^{(\sigma)}$ and $\chi_{\perp\perp\parallel}^{(\sigma)} = \chi_{\perp\parallel\perp}^{(\sigma)}$ are nonvanishing. This can be understood from the following qualitative picture: an electric field along α leads to an imbalance between the populations at $\pm\mathbf{k} \parallel \mathbf{E}$. Due to the spin polarization of the bands, see Fig. 2b, this imbalance directly translates into the spin polarization and, as a result, into the spin current. In this picture, no spin imbalance is expected at $\mathbf{E} \perp \alpha$, hence $\chi_{\parallel\perp\perp}^{(\sigma)} = 0$.

In passing, we note that combining a p -wave magnet with a regular metal makes it possible to achieve spin filtering with different conductances for spin-up and spin-down electrons. The filtering is observed for the orientation of the interface that does not respect the combined translation and time reversal symmetry of the p -wave magnet, i.e., α should have a component perpendicular to the interface, see the Supplemental Material [51].

Concluding remarks.— Our minimal lattice and effective models for p -wave magnets are given in Eqs. (1) and (2), respectively. The lattice model requires only four sites with rotated by $\pi/2$ between each site localized spins and is $\mathcal{T}\tau$ -symmetric, see Fig. 1a. While the rotating spin texture is similar to that in helimagnets, which can also exhibit p -wave spin-polarized electron bands [47, 50],

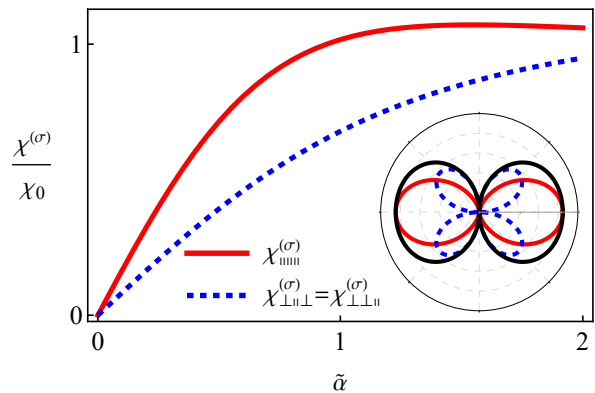


FIG. 4. The nontrivial components of the second-order spin response tensor $\chi_{ijl}^{(\sigma)}$ as a function of the spin-splitting parameter $\tilde{\alpha}$. The inset shows the dependence of the spin current components $j_{\sigma,\parallel}$ (solid red line), $j_{\sigma,\perp}$ (dashed blue line), and the magnitude of the current (solid black line) on the angle between \mathbf{E} and α at $\tilde{\alpha} = 1$. We use $\chi_0 = e^3 \tau^2 k_F / m$ with τ being relaxation time and set $\tilde{J} = 1.5$.

the p -wave symmetry in unconventional magnets is protected by the $\mathcal{T}\tau$ symmetry.

We used an effective model to describe the spin transport properties in heterostructures exemplified by the TMR and spin current responses. The characteristic dependence of the TMR on the relative angle between the spin-splitting vectors α in the magnets composing the heterostructures provides an experimentally viable way to identify p -wave magnets: the spin-flip necessary for the TMR is achieved by rotating one of the magnets by π rather than $\pi/2$ as in d -wave altermagnets. The relatively large magnitude of the TMR $\sim 100 - 200\%$ makes p -wave magnets promising for spintronic applications.

Similar to d -wave magnets [10], unconventional p -wave magnets allow for a spin current accompanied by an electric current. However, in the model at hand, there is no spin-splitter effect [10], where the spin current is perpendicular to the applied electric field.

The proposed model can readily address the transport properties of superconducting junctions and interaction effects in p -wave magnets. Indeed, as in helical and cycloidal magnets [56], the nontrivial spin texture of our model realizes synthetic spin-sectoral coupling, which could allow for Majorana bound states. Therefore, our model provides a playground to study the interplay of unconventional magnetism, superconductivity, and, after a model extension, topology [57].

Acknowledgments. Jeroen Danon is thanked for useful comments. The Research Council of Norway (RCN) supported this work through its Centres of Excellence funding scheme, project number 262633, "QuSpin", and RCN project number 323766.

* These authors contributed equally to this work

- [1] L.-D. Yuan, Z. Wang, J.-W. Luo, E. I. Rashba, and A. Zunger, Giant momentum-dependent spin splitting in centrosymmetric low- Z antiferromagnets, *Phys. Rev. B* **102**, 014422 (2020).
- [2] L. Šmejkal, J. Sinova, and T. Jungwirth, Emerging Research Landscape of Altermagnetism, *Phys. Rev. X* **12**, 040501 (2022).
- [3] L. Šmejkal, J. Sinova, and T. Jungwirth, Beyond Conventional Ferromagnetism and Antiferromagnetism: A Phase with Nonrelativistic Spin and Crystal Rotation Symmetry, *Phys. Rev. X* **12**, 031042 (2022).
- [4] I. Mazin and The PRX Editors, Editorial: Altermagnetism—A New Punch Line of Fundamental Magnetism, *Phys. Rev. X* **12**, 040002 (2022).
- [5] S. Hayami, Y. Yanagi, and H. Kusunose, Momentum-Dependent Spin Splitting by Collinear Antiferromagnetic Ordering, *J. Phys. Soc. Jpn.* **88**, 123702 (2019).
- [6] K.-H. Ahn, A. Hariki, K.-W. Lee, and J. Kuneš, Antiferromagnetism in RuO₂ as d -wave Pomeranchuk instability, *Phys. Rev. B* **99**, 184432 (2019).
- [7] L.-D. Yuan, Z. Wang, J.-W. Luo, and A. Zunger, Prediction of low- Z collinear and noncollinear antiferromagnetic compounds having momentum-dependent spin splitting even without spin-orbit coupling, *Phys. Rev. Mater.* **5**, 014409 (2021).
- [8] Y. Noda, K. Ohno, and S. Nakamura, Momentum-dependent band spin splitting in semiconducting MnO₂: A density functional calculation, *Phys. Chem. Chem. Phys.* **18**, 13294 (2016).
- [9] L. Šmejkal, A. B. Hellenes, R. González-Hernández, J. Sinova, and T. Jungwirth, Giant and Tunneling Magnetoresistance in Unconventional Collinear Antiferromagnets with Nonrelativistic Spin-Momentum Coupling, *Phys. Rev. X* **12**, 011028 (2022).
- [10] R. González-Hernández, L. Šmejkal, K. Výborný, Y. Yahagi, J. Sinova, T. Jungwirth, and J. Železný, Efficient electrical spin splitter based on nonrelativistic collinear antiferromagnetism, *Phys. Rev. Lett.* **126**, 127701 (2021).
- [11] S. Karube, T. Tanaka, D. Sugawara, N. Kadoguchi, M. Kohda, and J. Nitta, Observation of Spin-Splitter Torque in Collinear Antiferromagnetic RuO₂, *Phys. Rev. Lett.* **129**, 137201 (2022).
- [12] D.-F. Shao, S.-H. Zhang, M. Li, C.-B. Eom, and E. Y. Tsymbal, Spin-neutral currents for spintronics, *Nat. Commun.* **12**, 7061 (2021).
- [13] M. Naka, S. Hayami, H. Kusunose, Y. Yanagi, Y. Motome, and H. Seo, Spin current generation in organic antiferromagnets, *Nature communications* **10**, 4305 (2019).
- [14] X. Zhou, W. Feng, R.-W. Zhang, L. Šmejkal, J. Sinova, Y. Mokrousov, and Y. Yao, Crystal Thermal Transport in Altermagnetic RuO₂, *Phys. Rev. Lett.* **132**, 056701 (2024).
- [15] Q. Cui, B. Zeng, P. Cui, T. Yu, and H. Yang, Efficient spin seebeck and spin nernst effects of magnons in altermagnets, *Phys. Rev. B* **108**, L180401 (2023).
- [16] Q. Liu, J. Kang, P. Wang, W. Gao, Y. Qi, J. Zhao, and X. Jiang, Inverse Magnetocaloric Effect in Altermagnetic 2D Non-van der Waals FeX (X= S and Se) Semiconductors, *Adv. Funct. Mater.* , 2402080 (2024).
- [17] R. Hoyer, R. Jaeschke-Ubiergo, K.-H. Ahn, L. Šmejkal, and A. Mook, Spontaneous Crystal Thermal Hall Effect in Insulating Altermagnets (2024), [arxiv:2405.05090](https://arxiv.org/abs/2405.05090) [cond-mat].
- [18] A. Badura, W. H. Campos, V. K. Bharadwaj, I. Kounta, L. Michez, M. Petit, J. Rial, M. Leiviskä, V. Baltz, F. Krizek, D. Kriegner, J. Zemen, S. Telkamp, S. Sailler, M. Lammel, R. J. Ubiergo, A. B. Hellenes, R. González-Hernández, J. Sinova, T. Jungwirth, S. T. B. Goennenwein, L. Šmejkal, and H. Reichlova, Observation of the anomalous nernst effect in altermagnetic candidate Mn₅Si₃ (2024), [arxiv:2403.12929](https://arxiv.org/abs/2403.12929) [cond-mat].
- [19] J. A. Ouassou, A. Brataas, and J. Linder, dc josephson effect in altermagnets, *Phys. Rev. Lett.* **131**, 076003 (2023).
- [20] C. W. J. Beenakker and T. Vakhstel, Phase-shifted andreev levels in an altermagnet josephson junction, *Phys. Rev. B* **108**, 075425 (2023).
- [21] M. Papaj, Andreev reflection at the altermagnet-superconductor interface, *Phys. Rev. B* **108**, L060508 (2023).
- [22] C. Sun, A. Brataas, and J. Linder, Andreev reflection in altermagnets, *Phys. Rev. B* **108**, 054511 (2023).
- [23] D. Chakraborty and A. M. Black-Schaffer, Zero-field finite-momentum and field-induced superconductivity in altermagnets (2024), [arxiv:2309.14427](https://arxiv.org/abs/2309.14427) [cond-mat].
- [24] S. A. A. Ghorashi, T. L. Hughes, and J. Cano, Altermagnetic Routes to Majorana Modes in Zero Net Magnetization (2023), [arxiv:2306.09413](https://arxiv.org/abs/2306.09413) [cond-mat].
- [25] H. G. Giil and J. Linder, Superconductor-altermagnet memory functionality without stray fields, *Phys. Rev. B* **109**, 134511 (2024).
- [26] S. Das and A. Soori, Crossed Andreev reflection in altermagnets (2024), [arxiv:2402.08263](https://arxiv.org/abs/2402.08263) [cond-mat].
- [27] K. Mæland, B. Brekke, and A. Sudbø, Many-body effects on superconductivity mediated by double-magnon processes in altermagnets, *Phys. Rev. B* **109**, 134515 (2024).
- [28] H. G. Giil, B. Brekke, J. Linder, and A. Brataas, Quasiclassical theory of superconducting spin-splitter effects and spin-filtering via altermagnets (2024), [arxiv:2403.04851](https://arxiv.org/abs/2403.04851) [cond-mat].
- [29] B. Brekke, A. Brataas, and A. Sudbø, Two-dimensional altermagnets: Superconductivity in a minimal microscopic model, *Phys. Rev. B* **108**, 224421 (2023).
- [30] S.-B. Zhang, L.-H. Hu, and T. Neupert, Finite-momentum cooper pairing in proximitized altermagnets, *Nat. Commun.* **15**, 1801 (2024).
- [31] P. O. Sukhachov, E. W. Hodt, and J. Linder, Thermoelectric Effect in Altermagnet-Superconductor Junctions (2024), [arxiv:2404.10038](https://arxiv.org/abs/2404.10038) [cond-mat].
- [32] D. Zhu, Z.-Y. Zhuang, Z. Wu, and Z. Yan, Topological superconductivity in two-dimensional altermagnetic metals, *Phys. Rev. B* **108**, 184505 (2023).
- [33] S. Chourasia, A. Svetogorov, A. Kamra, and W. Belzig, Thermodynamic properties of a superconductor interfaced with an altermagnet (2024), [arxiv:2403.10456](https://arxiv.org/abs/2403.10456) [cond-mat].
- [34] The magnetic order in RuO₂ is debated [58, 59].
- [35] O. Fedchenko, J. Minár, A. Akashdeep, S. W. D'Souza, D. Vasilyev, O. Tkach, L. Odenbreit, Q. Nguyen, D. Kutnyakhov, N. Wind, L. Wenthaus, M. Scholz, K. Rossnagel, M. Hoesch, M. Aeschlimann, B. Stadtmüller, M. Kläui, G. Schönhense, T. Jungwirth, A. B. Hellenes, G. Jakob, L. Šmejkal, J. Sinova, and H.-J. Elmers, Ob-

- servation of time-reversal symmetry breaking in the band structure of altermagnetic RuO₂, *Sci. Adv.* **10**, eadj4883 (2024).
- [36] J. Krempaský, L. Šmejkal, S. D'Souza, M. Hajlaoui, G. Springholz, K. Uhlířová, F. Alarab, P. Constantinou, V. Strocov, D. Usanov, *et al.*, Altermagnetic lifting of kramers spin degeneracy, *Nature* **626**, 517 (2024).
- [37] T. Osumi, S. Souma, T. Aoyama, K. Yamauchi, A. Honma, K. Nakayama, T. Takahashi, K. Ohgushi, and T. Sato, Observation of a giant band splitting in altermagnetic MnTe, *Phys. Rev. B* **109**, 115102 (2024).
- [38] S. Reimers, L. Odenbreit, L. Šmejkal, V. N. Strocov, P. Constantinou, A. B. Hellenes, R. Jaeschke Ubierno, W. H. Campos, V. K. Bharadwaj, A. Chakraborty, *et al.*, Direct observation of altermagnetic band splitting in CrSb thin films, *Nat. Commun.* **15**, 2116 (2024).
- [39] M. Zeng, M.-Y. Zhu, Y.-P. Zhu, X.-R. Liu, X.-M. Ma, Y.-J. Hao, P. Liu, G. Qu, Y. Yang, Z. Jiang, K. Yamagami, M. Arita, X. Zhang, T.-H. Shao, Y. Dai, K. Shimada, Z. Liu, M. Ye, Y. Huang, Q. Liu, and C. Liu, Observation of Spin Splitting in Room-Temperature Metallic Antiferromagnet CrSb (2024), [arxiv:2405.12679](https://arxiv.org/abs/2405.12679) [cond-mat].
- [40] J. Ding, Z. Jiang, X. Chen, Z. Tao, Z. Liu, J. Liu, T. Li, J. Liu, Y. Yang, R. Zhang, L. Deng, W. Jing, Y. Huang, Y. Shi, S. Qiao, Y. Wang, Y. Guo, D. Feng, and D. Shen, Large band-splitting in *g*-wave type altermagnet CrSb (2024), [arxiv:2405.12687](https://arxiv.org/abs/2405.12687) [cond-mat].
- [41] W. Brinkman and R. J. Elliott, Theory of spin-space groups, *Proc. R. Soc. Lond. A* **294**, 343 (1966).
- [42] A. Corticelli, R. Moessner, and P. A. McClarty, Spin-space groups and magnon band topology, *Phys. Rev. B* **105**, 064430 (2022).
- [43] Z. Xiao, J. Zhao, Y. Li, R. Shindou, and Z.-D. Song, Spin Space Groups: Full Classification and Applications (2023), [arxiv:2307.10364](https://arxiv.org/abs/2307.10364) [cond-mat].
- [44] X. Chen, J. Ren, Y. Zhu, Y. Yu, A. Zhang, P. Liu, J. Li, Y. Liu, C. Li, and Q. Liu, *Enumeration and representation theory of spin space groups* (2023).
- [45] S.-W. Cheong and F.-T. Huang, Altermagnetism with non-collinear spins, *npj Quantum Mater.* **9**, 13 (2024).
- [46] D. K. Singh, S.-W. Cheong, and J. Guo, Altermagnetism in NiSi with non-collinear spins (2024), [arxiv:2402.17451](https://arxiv.org/abs/2402.17451) [cond-mat].
- [47] Y. B. Kudasov, Topological band structure due to modified kramers degeneracy for electrons in a helical magnetic field, *Phys. Rev. B* **109**, L140402 (2024).
- [48] A. B. Hellenes, T. Jungwirth, J. Sinova, and L. Šmejkal, Unconventional p-wave magnets (2024), [arxiv:2309.01607](https://arxiv.org/abs/2309.01607) [cond-mat].
- [49] G. Chen, M. Khosravian, J. L. Lado, and A. Ramires, Designing spin-textured flat bands in twisted graphene multilayers via helimagnet encapsulation, *2D Mater.* **9**, 024002 (2022), [arXiv:2109.13130](https://arxiv.org/abs/2109.13130).
- [50] A. H. Mayo, D.-A. Deaconu, H. Masuda, Y. Nii, H. Takahashi, R. V. Belosludov, S. Ishiwata, M. S. Bahramy, and Y. Onose, Band-asymmetry-driven nonreciprocal electronic transport in a helimagnetic semimetal α -EuP₃ (2024), [arxiv:2404.13856](https://arxiv.org/abs/2404.13856) [cond-mat].
- [51] See Supplemental Material for additional numerical results and details of the tunneling magnetoresistance, spin filtering, and bulk transport calculations..
- [52] E. Y. Tsymlal, O. N. Mryasov, and P. R. LeClair, Spin-dependent tunnelling in magnetic tunnel junctions, *J. Phys. Condens. Matter* **15**, R109 (2003).
- [53] Similar to the helical orientation in helimagnets [60], the direction of the spin-splitting vector α may be controllable via current pulses.
- [54] H. Katsura, N. Nagaosa, and A. V. Balatsky, Spin current and magnetoelectric effect in noncollinear magnets, *Phys. Rev. Lett.* **95**, 057205 (2005).
- [55] E. I. Rashba, Spin currents in thermodynamic equilibrium: The challenge of discerning transport currents, *Phys. Rev. B* **68**, 241315 (2003).
- [56] S. Rex, I. V. Gornyi, and A. D. Mirlin, Majorana modes in emergent-wire phases of helical and cycloidal magnet-superconductor hybrids, *Phys. Rev. B* **102**, 224501 (2020).
- [57] The topology of electron band structures in helimagnets was recently studied in Ref. [47].
- [58] M. Hiraiishi, H. Okabe, A. Koda, R. Kadono, T. Muroi, D. Hirai, and Z. Hiroi, Nonmagnetic Ground State in RuO₂ Revealed by Muon Spin Rotation, *Phys. Rev. Lett.* **132**, 166702 (2024).
- [59] P. Keßler, L. Garcia-Gassull, A. Suter, T. Prokscha, Z. Salman, D. Khalyavin, P. Manuel, F. Orlandi, I. I. Mazin, R. Valenti, and S. Moser, Absence of magnetic order in RuO₂: Insights from μ SR spectroscopy and neutron diffraction (2024), [arxiv:2405.10820](https://arxiv.org/abs/2405.10820) [cond-mat].
- [60] J. Masell, X. Yu, N. Kanazawa, Y. Tokura, and N. Nagaosa, Combing the helical phase of chiral magnets with electric currents, *Phys. Rev. B* **102**, 180402 (2020), [arXiv:2007.03414](https://arxiv.org/abs/2007.03414).

Supplemental Material

Minimal models and transport properties of unconventional p -wave magnets

CONTENTS

I. Effective model	1
A. Minimal lattice model	1
B. Effective model	1
C. Topology	3
II. Tunneling magnetoresistance (TMR)	3
1. Bilayer	4
2. Planar junction	5
III. Spin filtering	5
IV. Nonlinear transport	8
A. First-order response	9
B. Second-order response	10
References	11

I. EFFECTIVE MODEL

In this section, we provide additional details of our lattice and effective models in Eqs. (1) and (2) in the main text.

A. Minimal lattice model

The lattice tight-binding model in Eq. (1) and Fig. 1a in the main text can be diagonalized in the reciprocal space. We Fourier transform the electron operators and find

$$H_e = \sum_{k, \ell, \ell', \sigma, \sigma'} c_{\ell, k, \sigma}^\dagger (\mathcal{H}_k)_{\ell, \ell', \sigma, \sigma'} c_{\ell', k, \sigma'}, \quad (1)$$

where ℓ and ℓ' run over the four sites and in the magnetic unit cell, σ and σ' run over the spin degree of freedom and k runs over the first Brillouin zone. The matrix form of the Hamiltonian is

$$\mathcal{H}_k = \begin{pmatrix} -\mu & J_{\text{sd}} & -te^{ik\delta} & 0 & 0 & 0 & -t^*e^{-ik\delta} & 0 \\ J_{\text{sd}} & -\mu & 0 & -te^{ik\delta} & 0 & 0 & 0 & -t^*e^{-ik\delta} \\ -t^*e^{ik\delta} & 0 & -\mu & -iJ_{\text{sd}} & -te^{ik\delta} & 0 & 0 & 0 \\ 0 & -t^*e^{-ik\delta} & iJ_{\text{sd}} & -\mu & 0 & -te^{ik\delta} & 0 & 0 \\ 0 & 0 & -t^*e^{-ik\delta} & 0 & -\mu & -J_{\text{sd}} & -te^{ik\delta} & 0 \\ 0 & 0 & 0 & -t^*e^{-ik\delta} & -J_{\text{sd}} & -\mu & 0 & -te^{ik\delta} \\ -te^{ik\delta} & 0 & 0 & 0 & -t^*e^{-ik\delta} & 0 & -\mu & iJ_{\text{sd}} \\ 0 & -te^{ik\delta} & 0 & 0 & 0 & -t^*e^{-ik\delta} & -iJ_{\text{sd}} & -\mu \end{pmatrix}, \quad (2)$$

where J_{sd} is the coupling between localized and itinerant electron spins, t is the nearest-neighbor hopping parameter, δ is the nearest-neighbor distance, and μ is the chemical potential.

B. Effective model

The effective Hamiltonian in the main text, Eq. (2), has a real space interpretation based on the main text's effective lattice in Fig. 2(a). It can be interpreted as real space hopping within two

sectors. It is block diagonal in terms of the two sectors

$$H_{\text{eff}} = \begin{pmatrix} H_{\text{sector}_1} & 0 \\ 0 & H_{\text{sector}_2} \end{pmatrix}, \quad (3)$$

where

$$H_{\text{sector}_1} = \begin{pmatrix} \sum_{i \in (x,y)} [-2t \cos(k_i a) + \alpha_i \sin(k_i a)] - \mu & J_{\text{sd}} \\ J_{\text{sd}} & \sum_{i \in (x,y)} [-2t \cos(k_i a) - \alpha_i \sin(k_i a)] - \mu \end{pmatrix} \quad (4)$$

and

$$H_{\text{sector}_2} = \begin{pmatrix} \sum_{i \in (x,y)} [-2t \cos(k_i a) + \alpha_i \sin(k_i a)] - \mu & -J_{\text{sd}} \\ -J_{\text{sd}} & \sum_{i \in (x,y)} [-2t \cos(k_i a) - \alpha_i \sin(k_i a)] - \mu \end{pmatrix}. \quad (5)$$

The dispersion relation and the spin polarization in the model (3) are given in Eqs. (3) and (4) in the main text, which, for convenience, we reproduce below

$$\varepsilon_{\pm} = -2t [\cos(k_x a) + \cos(k_y a)] \pm \sqrt{J_{\text{sd}}^2 + [\alpha_x \sin(k_x a) + \alpha_y \sin(k_y a)]^2} \quad (6)$$

and

$$\langle S_z \rangle = \pm 2 \frac{\alpha_x \sin(k_x a) + \alpha_y \sin(k_y a)}{\sqrt{J_{\text{sd}}^2 + [\alpha_x \sin(k_x a) + \alpha_y \sin(k_y a)]^2}}. \quad (7)$$

The spin polarization (7) is generalized to the arbitrary direction of α .

While each sector has a nontrivial spin texture with nonzero spin polarization along different axes, the polarization components $\langle S_x \rangle$ and $\langle S_y \rangle$ vanish after the summation over both sectors.

We present the constant energy contours with the spin polarization in Fig. 1.

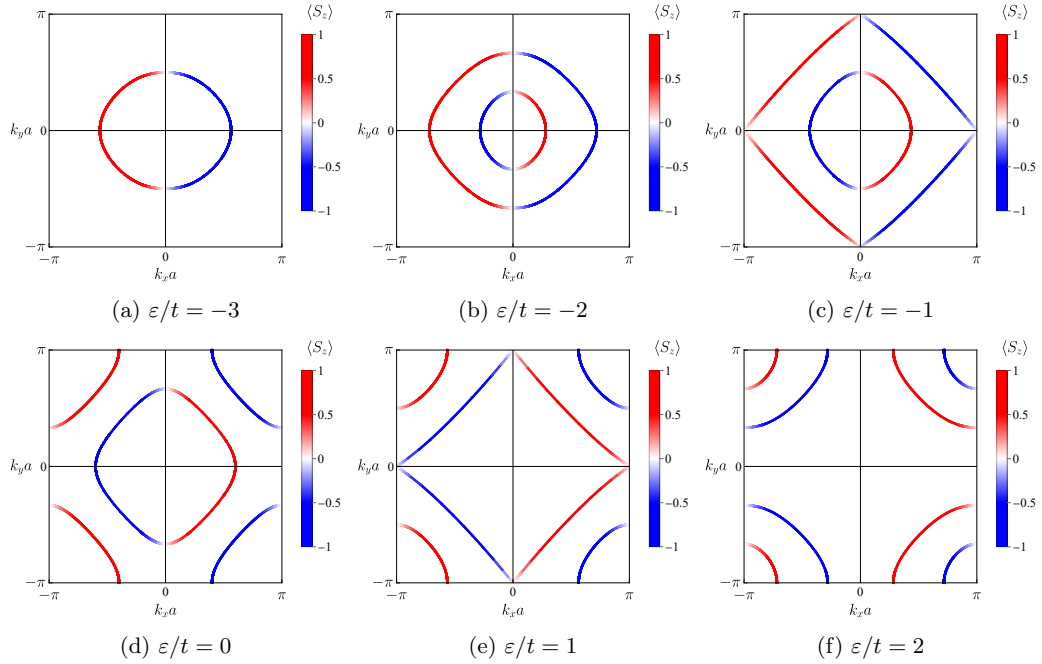


FIG. 1: The constant energy contours at different values of energy ε . The spin polarization $\langle S_z \rangle$ is shown in red and blue colors. We use Eqs. (6) and (7) for the energy spectrum and the spin polarization, respectively. In all panels, we fix $J_{\text{sd}}/t = \alpha/t = 1$.

C. Topology

The proposed model can be generalized to include nontrivial topology. In the case of the effective model, momentum-dependent sd-coupling is sufficient.

Let us illustrate this in a 1D version of our model. For example, modifying $J_{\text{sd}} \rightarrow J_{\text{sd}} \cos(k_x a)$ in Eqs. (3), (4), and (5) allows for a nontrivial winding number per sector

$$\nu_\eta = \frac{1}{2\pi} \int dk_x \psi_\eta^\dagger i\sigma_y \partial_{k_x} \psi_\eta = -\frac{\eta}{2\pi} \sum_{\pm} \int dk_x \frac{J_{\text{sd}} \alpha \cos k_x a}{J_{\text{sd}}^2 + \alpha^2 \sin^2(k_x a)} = \eta, \quad (8)$$

where ψ_η is the eigenstate for each of the sectors $\eta = \pm$. The winding number depends nontrivially on J_{sd} and α :

$$\nu_\eta = \begin{cases} -1 & \sqrt{\left| \frac{\eta J_{\text{sd}} - \alpha}{\eta J_{\text{sd}} + \alpha} \right|} < 1 \\ 1 & \sqrt{\left| \frac{\eta J_{\text{sd}} - \alpha}{\eta J_{\text{sd}} + \alpha} \right|} \geq 1 \end{cases}. \quad (9)$$

Let us consider a domain wall at $x = 0$ with $\alpha > 0$ at $x > 0$ and $\alpha < 0$ at $x < 0$; the coefficient J_{sd} is assumed to be the same. Then, according to Eq. (9), the winding numbers ν_η are different at $x > 0$ and $x < 0$. Due to the bulk-boundary correspondence, the difference between winding numbers signifies the presence of two (per sector) bound states at the interface. If sectors do not intermix, there should be four topological states.

II. TUNNELING MAGNETORESISTANCE (TMR)

This section calculates the tunneling magnetoresistance (TMR) in unconventional p -wave magnets. We focus on two types of junctions composed of 2D p -wave magnets: (i) a bilayer and (ii) a planar junction.

To make an analytical advance, we linearize the effective model in Eqs. (3)–(5) around the Γ point:

$$H_\eta^{(\text{lin})}(\mathbf{k}) = \left(\frac{k^2}{2m} - \mu \right) \sigma_0 + (\boldsymbol{\alpha}' \cdot \mathbf{k}) \sigma_z + \eta J_{\text{sd}} \sigma_x, \quad (10)$$

where $1/m = 2ta^2$, $\boldsymbol{\alpha}' = a\boldsymbol{\alpha}$, and $\eta = \pm$; to simplify the notations, we will omit the prime and use $\boldsymbol{\alpha}$ instead of $\boldsymbol{\alpha}'$.

We find it convenient to use dimensionless variables:

$$\tilde{J} = \frac{J_{\text{sd}}}{\mu}, \quad \tilde{\boldsymbol{\alpha}} = \frac{2m\boldsymbol{\alpha}}{k_F}, \quad \tilde{k} = \frac{k}{k_F} \quad (11)$$

with $k_F = \sqrt{2m\mu}$.

The tunneling current between the p -wave magnets reads [1, 2]:

$$I(V) = 4e\pi^3 \sum_{\eta=\pm} \int_{-\infty}^{\infty} d\omega \sum_{\mathbf{k}, \mathbf{p}} |T_{\mathbf{p}, \mathbf{k}}|^2 \text{Tr} \{ \text{Im} \{ G_{1; \eta}(\omega; \mathbf{p}) \} \text{Im} \{ G_{2; \eta}(\omega - eV; \mathbf{k}) \} [f_2(\omega - eV) - f_1(\omega)] \}. \quad (12)$$

Here, $G_{i; \eta}(\omega; \mathbf{p})$ is the retarded Green's function of the i -th magnet, $T_{\mathbf{p}, \mathbf{k}}$ is the tunneling coefficient, $f_i(\omega)$ is the Fermi-Dirac distribution function, and eV is the voltage bias between the magnets.

The tunneling coefficient for a bilayer preserves in-plane momenta: $|T_{\mathbf{p}, \mathbf{k}}|^2 = T^2 \delta_{\mathbf{p}, \mathbf{k}}$. In the case of interfaces, only the momentum components along the interface are conserved: $|T_{\mathbf{p}, \mathbf{k}}|^2 = T^2 \delta_{p_\parallel, k_\parallel} / L$ with L being the size of the interface.

The Green's function is defined as

$$G_{i; \eta}(\omega; \mathbf{k}) = \frac{1}{\omega + i0^+ - H_\eta(\mathbf{k})} = \frac{(\tilde{\omega} + \tilde{k}^2 - 1) \sigma_0 + \eta \tilde{J}_i \sigma_x + (\tilde{\boldsymbol{\alpha}}_i \cdot \tilde{\mathbf{k}}) \sigma_z}{(\tilde{\omega} + i0^+ + \tilde{k}^2 - 1)^2 - \tilde{J}_i^2 - (\tilde{\boldsymbol{\alpha}}_i \cdot \tilde{\mathbf{k}})^2}, \quad (13)$$

where we used the Hamiltonian (10) in the second expression.

The imaginary part is straightforwardly obtained by using the Sokhotski–Plemelj theorem,

$$\begin{aligned} \text{Im} \{G_{i;\eta}(\omega; \mathbf{k})\} &= -\pi \text{sgn}(\tilde{\omega} + \tilde{k}^2 - 1) \delta\left(\left(\tilde{\omega} + \tilde{k}^2 - 1\right)^2 - \tilde{J}_i^2 - \left(\tilde{\boldsymbol{\alpha}}_i \cdot \tilde{\mathbf{k}}\right)^2\right) \\ &\times \left[\left(\tilde{\omega} + \tilde{k}^2 - 1\right) \sigma_0 + \eta \tilde{J}_i \sigma_x + \left(\tilde{\boldsymbol{\alpha}}_i \cdot \tilde{\mathbf{k}}\right) \sigma_z\right]. \end{aligned} \quad (14)$$

We focus on the differential conductance $G = dI/dV$, assume the low-temperature limit $T \rightarrow 0$, and consider the limit of small voltage biases $|eV| \ll \mu$. This allows us to simplify the expression for the differential conductance:

$$G = \frac{dI}{dV} = 4e\pi^3 \sum_{\eta=\pm} \sum_{\mathbf{k}, \mathbf{p}} |T_{\mathbf{p}, \mathbf{k}}|^2 \text{Tr}\{\text{Im}\{G_{1;\eta}(0; \mathbf{p})\} \text{Im}\{G_{2;\eta}(0; \mathbf{k})\}\}. \quad (15)$$

1. Bilayer

In the bilayer, the differential conductance (15) is rewritten as

$$\begin{aligned} G(\theta_\alpha) &= 4e\pi^3 \sum_{\eta=\pm} \int \frac{d^2\mathbf{k}}{(2\pi)^2} T^2 \text{Tr}\{\text{Im}\{G_{1;\eta}(0; \mathbf{k})\} \text{Im}\{G_{2;\eta}(0; \mathbf{k})\}\} \\ &= e\pi^2 k_F^2 T^2 \int_0^{2\pi} \frac{d\theta}{2\pi} \sum_{\tilde{k}_\pm} \delta\left(\left(\tilde{k}_\pm^2 - 1\right)^2 - \tilde{J}_2^2 - \tilde{\alpha}_2^2 \tilde{k}_\pm^2 \cos^2\left(\frac{\theta - \theta_\alpha}{2}\right)\right) \\ &\times \left[\left(\tilde{k}_\pm^2 - 1\right)^2 + \tilde{J}_1 \tilde{J}_2 + \tilde{k}_\pm^2 \frac{\tilde{\alpha}_1 \tilde{\alpha}_2}{2} (\cos\theta + \cos\theta_\alpha)\right], \end{aligned} \quad (16)$$

where we used Eq. (14), defined

$$\tilde{k}_\pm^2 = 1 + \frac{\tilde{\alpha}_1^2}{2} \cos^2\left(\frac{\theta + \theta_\alpha}{2}\right) \pm \sqrt{\tilde{J}_1^2 + \tilde{\alpha}_1^2 \cos^2\left(\frac{\theta + \theta_\alpha}{2}\right) \left[1 + \frac{\tilde{\alpha}_1^2}{4} \cos^2\left(\frac{\theta + \theta_\alpha}{2}\right)\right]}, \quad (17)$$

and introduced the angle θ_α between the spin-splitting vectors in two layers, $\boldsymbol{\alpha}_1$ and $\boldsymbol{\alpha}_2$.

The δ -function in Eq. (16) is treated as a Lorentzian, $\delta(x) \rightarrow \delta_\Gamma(x)$:

$$\delta_\Gamma(x) = \frac{1}{\pi} \frac{\Gamma}{x^2 + \Gamma^2}. \quad (18)$$

As in the main text, see Eq. (6) there, we define the TMR as

$$\text{TMR} = \frac{G(\theta_\alpha) - G(\theta_\alpha + \pi)}{G(\theta_\alpha + \pi)}. \quad (19)$$

We present the TMR for the bilayer in Fig. 2. The strong dependence on \tilde{J}_2 shown in Fig. 2 originates primarily from the mismatch of the Fermi surfaces rather than the spin polarization. As one can see from Figs. 2(a) and 2(b), perfect matching of parameters \tilde{J} may not be needed to achieve large TMR. However, matching the spin-splitting vectors is desirable.

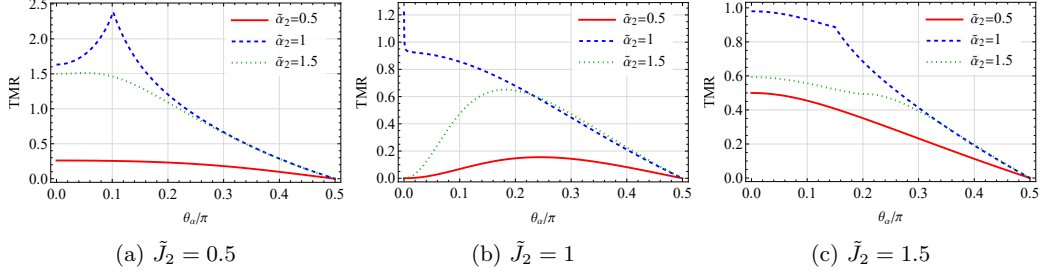


FIG. 2: TMR as a function of the relative angle θ_α between the spin-splitting vectors α_1 and α_2 in two layers of the bilayer. In all panels, $\tilde{\alpha}_1 = 1$, $\tilde{J}_1 = 1$, and $\tilde{\Gamma} = 10^{-3}$.

2. Planar junction

In the case of the planar junction, we have the following expression for the conductance (15):

$$\begin{aligned}
 G(\theta_{\alpha,1}, \theta_{\alpha,2}) &= 4e\pi^3 \sum_{\eta=\pm} \int \frac{d^2\mathbf{k}}{(2\pi)^2} \int \frac{dp_\perp}{2\pi} T^2 \text{Tr} \{ \text{Im} \{ G_{1,\eta}(0; \mathbf{k}) \} \text{Im} \{ G_{2,\eta}(0; p_\perp, k_\parallel) \} \} \\
 &= e\pi^3 T^2 k_F^3 \int_0^{2\pi} \frac{d\theta_1}{2\pi} \int_0^\infty \tilde{k} d\tilde{k} \int_{-\infty}^\infty d\tilde{p}_\perp \text{sgn}(\tilde{k}^2 - 1) \text{sgn}(\tilde{k}^2 \sin^2 \theta_1 + \tilde{p}_\perp^2 - 1) \\
 &\times \delta\left(\left(\tilde{k}^2 - 1\right)^2 - \tilde{J}_1^2 - \tilde{k}^2 \tilde{\alpha}_1^2 (\cos \theta_1 \cos \theta_{\alpha,1} + \sin \theta_1 \sin \theta_{\alpha,1})^2\right) \\
 &\times \delta\left(\left(\tilde{k}^2 \sin^2 \theta_1 + \tilde{p}_\perp^2 - 1\right)^2 - \tilde{J}_2^2 - \tilde{\alpha}_2^2 (\tilde{p}_\perp \cos \theta_{\alpha,2} + \tilde{k} \sin \theta_1 \sin \theta_{\alpha,2})^2\right) \\
 &\times \left[\tilde{J}_1 \tilde{J}_2 + (\tilde{k}^2 - 1) (\tilde{k}^2 \sin^2 \theta + \tilde{p}_\perp^2 - 1) \right. \\
 &\left. + \tilde{k} \tilde{\alpha}_1 \tilde{\alpha}_2 (\cos \theta_1 \cos \theta_{\alpha,1} + \sin \theta_1 \sin \theta_{\alpha,1}) (\tilde{p}_\perp \cos \theta_{\alpha,2} + \tilde{k} \sin \theta_1 \sin \theta_{\alpha,2}) \right], \quad (20)
 \end{aligned}$$

where the angles are calculated with respect to the normal to the junction. The δ -functions allow us to straightforwardly integrate over \tilde{k} and \tilde{p}_\perp ; the integral over θ_1 is taken numerically.

Since there is a preferred direction in a planar interface, the junction cannot be characterized by a single angle θ_α . Then, the definition of the TMR (19) is modified as

$$\text{TMR} = \frac{G(\theta_{\alpha,1}, \theta_{\alpha,2}) - G(\theta_{\alpha,1}, \theta_{\alpha,2} + \pi)}{G(\theta_{\alpha,1}, \theta_{\alpha,2} + \pi)}, \quad (21)$$

cf. Eq. (19).

We present the TMR for the planar interface in Fig. 3. Compared to the bilayer, see Fig. 2, the TMR in the planar interface is less sensitive to the mismatch of model parameters and can show larger values of the TMR.

III. SPIN FILTERING

Let us show that p -wave magnets allow for spin filtering where the differential conductances for spin-up and spin-down particles differ.

We consider a planar interface between an unconventional p -wave magnet and a regular metal. The Hamiltonian for the interface is

$$H_\eta(x, k_y) = \left(-\frac{\nabla_x^2}{2m} + \frac{k_\parallel^2}{2m} - \mu \right) \sigma_0 + \left[-\frac{i}{2} \{ \alpha_x(x), \nabla_x \} + \alpha_y(x) k_y \right] \sigma_z + \eta J_{\text{sd}}(x) \sigma_x + U(x) \sigma_0, \quad (22)$$

where $\alpha(x) = \alpha \Theta(x)$ and $J_{\text{sd}}(x) = J_{\text{sd}} \Theta(x)$ with $\Theta(x)$ being the unit-step function; the barrier at the interface is modeled as $U(x) = U \delta(x)$ [3]. For definiteness, we fixed x - and y -axes to be perpendicular

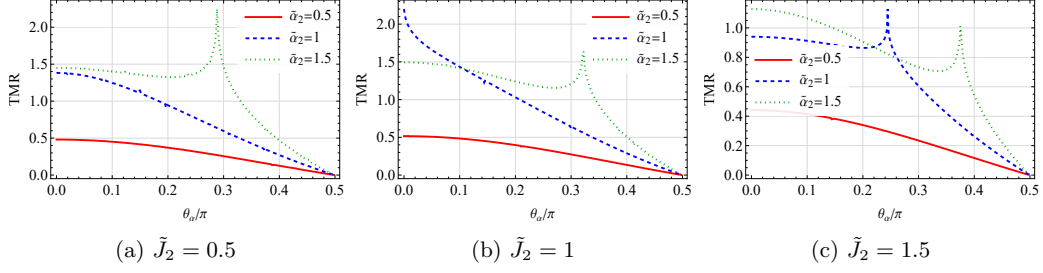


FIG. 3: TMR as a function of the angle $\theta_\alpha = \theta_{\alpha,2} - \theta_{\alpha,1}$ between the spin-splitting vectors α_1 and α_2 in two magnets of the planar junction. We fixed $\theta_{\alpha,1} = \pi/2$ in Eqs. (20) and (21). In all panels, $\tilde{J}_1 = 1$ and $\tilde{\alpha}_1 = 1$.

and parallel to the interface, respectively. Note that the form of the term $\{\alpha_x(x), \nabla_x\}$ with $\{\dots, \dots\}$ being the anticommutator is enforced by the hermiticity of the Hamiltonian.

We determine the differential conductance on the metallic part of the junction assuming impinging electrons with the spin projection s via the standard formulas:

$$G_{e;s}(V) = -e^2 L^3 \sum_{\eta=\pm} \int \frac{d\mathbf{k}}{(2\pi)^2} j_{e;\eta,s} f'(\varepsilon - eV) = -e^2 L^3 \sum_{\eta=\pm} \int \frac{dk_y}{(2\pi)^2} \int d\varepsilon \frac{\partial k_x}{\partial \varepsilon} j_{e;\eta,s} f'(\varepsilon - eV) \quad (23)$$

for the electric conductance and

$$G_{\sigma;s}(V) = -e^2 L^3 \sum_{\eta=\pm} \int \frac{dk_y}{(2\pi)^2} \int d\varepsilon \frac{\partial k_x}{\partial \varepsilon} j_{\sigma;\eta,s} f'(\varepsilon - eV) \quad (24)$$

for the spin conductance. Here, prime denotes the derivative with respect to the argument. The summation over the spin projections is performed in the full electric and spin conductances. The electric and spin currents used in Eqs. (23) and (24) are

$$j_{e;\eta,s} = \frac{1}{2L^2} \text{Re} \left\{ \psi_{\eta,s}^\dagger \overleftrightarrow{v}_x \psi_{\eta,s} \right\}, \quad (25)$$

$$j_{\sigma;\eta,s} = \frac{1}{2L^2} \text{Re} \left\{ \psi_{\eta,s}^\dagger \sigma_z \overleftrightarrow{v}_x \psi_{\eta,s} \right\}, \quad (26)$$

respectively. For the current in the metallic part of the junction, $\hat{v}_x = -i\nabla_x/m$, and $\psi_{\eta,s}$ denote the scattering states. The scattering states for impinging spin-up and spin-down particles are:

$$\psi_{\eta,+}(x < 0) = e^{ik_x x + ik_y y} \begin{pmatrix} 1 \\ 0 \end{pmatrix} + r_{1,\eta,+} e^{-ik_x x - ik_y y} \begin{pmatrix} 1 \\ 0 \end{pmatrix} + r_{2,\eta,+} e^{-ik_x x - ik_y y} \begin{pmatrix} 0 \\ 1 \end{pmatrix}, \quad (27)$$

$$\psi_{\eta,+}(x > 0) = t_{1,\eta,+} e^{iq_{x,+} x + ik_y y} \psi_{\eta}(q_{x,+},+) + t_{2,\eta,+} e^{iq_{x,+} x + ik_y y} \psi_{\eta}(q_{x,+},-) \quad (28)$$

and

$$\psi_{\eta,-}(x < 0) = e^{ik_x x + ik_y y} \begin{pmatrix} 0 \\ 1 \end{pmatrix} + r_{1,\eta,-} e^{-ik_x x - ik_y y} \begin{pmatrix} 1 \\ 0 \end{pmatrix} + r_{2,\eta,-} e^{-ik_x x - ik_y y} \begin{pmatrix} 0 \\ 1 \end{pmatrix}, \quad (29)$$

$$\psi_{\eta,-}(x > 0) = t_{1,\eta,-} e^{iq_{x,+} x + ik_y y} \psi_{\eta}(q_{x,+},+) + t_{2,\eta,-} e^{iq_{x,+} x + ik_y y} \psi_{\eta}(q_{x,+},-) \quad (30)$$

respectively. Here, $k_x = k_F \sqrt{\tilde{\varepsilon} - \tilde{k}_y^2}$,

$$\psi_{\eta}(k_x) = \frac{|\tilde{\varepsilon} - \tilde{k}^2 + (\tilde{\alpha} \cdot \tilde{\mathbf{k}})|}{\sqrt{[\tilde{\varepsilon} - \tilde{k}^2 + (\tilde{\alpha} \cdot \tilde{\mathbf{k}})]^2 + \tilde{J}^2}} \begin{pmatrix} 1 \\ \frac{\eta \tilde{J}}{\tilde{\varepsilon} - \tilde{k}^2 + (\tilde{\alpha} \cdot \tilde{\mathbf{k}})} \end{pmatrix} \quad (31)$$

and $q_{x,s_1,s_2} = k_F \tilde{q}_{x,s_1,s_2}$ with

$$\alpha_y = 0: \quad \tilde{q}_{x,s_1,s_2} = s_1 \left\{ \tilde{\varepsilon} + \frac{\tilde{\alpha}_x^2}{2} - \tilde{k}_y^2 + s_2 \sqrt{\tilde{J}^2 + \tilde{\alpha}_x^2 \left(\frac{\tilde{\alpha}_x^2}{4} + \tilde{\varepsilon} - \tilde{k}_y^2 \right)} \right\}^{1/2}, \quad (32)$$

$$\alpha_x = 0: \quad \tilde{q}_{x,s_1,s_2} = s_1 \left\{ \tilde{\varepsilon} + 1 - \tilde{k}_y^2 + s_2 \sqrt{\tilde{J}^2 + \tilde{\alpha}_y^2 \tilde{k}_y^2} \right\}^{1/2}. \quad (33)$$

The wave vectors \tilde{q}_{x,s_1,s_2} are obtained from

$$\tilde{\varepsilon} = \tilde{q}^2 \pm \sqrt{\tilde{J}^2 + (\tilde{\alpha} \cdot \tilde{\mathbf{q}})^2}. \quad (34)$$

The roots are cumbersome for a generic orientation of α .

Note that since the Hamiltonian (22) is not diagonal in the spin space, we include the reflected waves of different spin polarizations and introduce two reflection coefficients: one ($r_{1,\eta,+}$ or $r_{2,\eta,-}$) corresponds to the reflection without the spin-flip and the other ($r_{2,\eta,+}$ or $r_{1,\eta,-}$) describes the spin-flip process.

The boundary conditions for the planar interface are

$$x = 0 : \quad \psi_{\eta,s}(x > 0) = \psi_{\eta,s}(x < 0), \quad (35)$$

$$x = 0 : \quad \partial_x \psi_{\eta,s}(x > 0) - \partial_x \psi_{\eta,s}(x < 0) = \left(Z - i \frac{\tilde{\alpha}_x}{2} \sigma_z \right) \psi_{\eta,s}(x > 0), \quad (36)$$

where the dimensionless parameter $Z = 2mU/k_F$ quantifies the strength of the potential barrier between the metal and the p -wave magnet. The last term in the parentheses in Eq. (36) originates from the term $-\frac{i}{2} \{ \alpha_x \Theta(x), \nabla_x \}$ in Eq. (22).

Substituting Eqs. (27), (28), (29), and (30) into Eqs. (25) and (26), as well as assuming the zero-temperature limit, we obtain the following electric (23) and spin (24) conductances:

$$\begin{aligned} G_e(V) &= e^2 L \sum_{\eta,s=\pm} \int \frac{dk_y}{(2\pi)^2} \int d\varepsilon (1 - |r_{1,s}|^2 - |r_{2,s}|^2) \delta(\varepsilon - \mu - eV) \\ &= \frac{\tilde{G}_Q}{2} \sum_{\eta,s=\pm} \int d\tilde{k}_y (1 - |r_{1,s}|^2 - |r_{2,s}|^2) \Big|_{\tilde{\varepsilon}=eV/\mu+1} \end{aligned} \quad (37)$$

and

$$\begin{aligned} G_\sigma(V) &= e^2 L \sum_{\eta,s=\pm} \int \frac{dk_y}{(2\pi)^2} \int d\varepsilon (s - |r_{1,s}|^2 + |r_{2,s}|^2) \delta(\varepsilon - \mu - eV) \\ &= \frac{\tilde{G}_Q}{2} \sum_{\eta,s=\pm} \int d\tilde{k}_y (s - |r_{1,s}|^2 + |r_{2,s}|^2) \Big|_{\tilde{\varepsilon}=eV/\mu+1}. \end{aligned} \quad (38)$$

Here, $\tilde{G}_Q = G_Q k_F L / (2\pi)$ with $G_Q = e^2 / \pi$. To quantify the spin filtering, we introduce the following conductance asymmetry:

$$\Delta G(V) = \frac{G_{e,\downarrow}(V) - G_{e,\uparrow}(V)}{G_{e,\uparrow}(V) + G_{e,\downarrow}(V)}. \quad (39)$$

We show the electric and spin conductance as well as the anisotropy (39) for the spin-splitting vector along the interface ($\alpha_y = 0$) in Fig. 4 at $\tilde{J} = 1$ (solid lines) and $\tilde{J} = 0.9$ (dashed lines), respectively. As one can see, the main effect of a smaller \tilde{J} is to reduce the voltage onset needed for a nontrivial conductance. The onset, i.e., the value of the voltage bias that should be reached for a nonzero conductance, is determined by requiring the wave vectors of electrons in the magnet to be real $\text{Re} \{ \tilde{q}_{x,+s_2} \} \geq 0$, i.e., there should be propagating electrons in the magnet. For the threshold, it is sufficient to consider the shortest trajectories and set $\tilde{k}_y = 0$. Then, by using Eq. (32), we determine the threshold

$$eV_{\text{cr}} = |J_{\text{sd}}| - \mu. \quad (40)$$

Note that \tilde{q}_{x,s_1,s_2} can be found exactly at $\tilde{k}_y = 0$. It is given by Eq. (32) at $\tilde{k}_y = 0$ and does not depend on α_y .

In contrast to the spin conductance, shown in Fig. 4(b), which is determined by the spin-splitting vector α , the electric conductance shown in Fig. 4(a) demonstrates negligible dependence on α . The conductance asymmetry (39) and, as a result, the spin filtering is maximal near the threshold and gradually decays with the bias eV .

The barrier strength Z suppresses the conductance and leads to a higher sensitivity of G_e to the spin-splitting vector; see the corresponding conductances in Fig. 5 for a relatively high $Z = 10$.

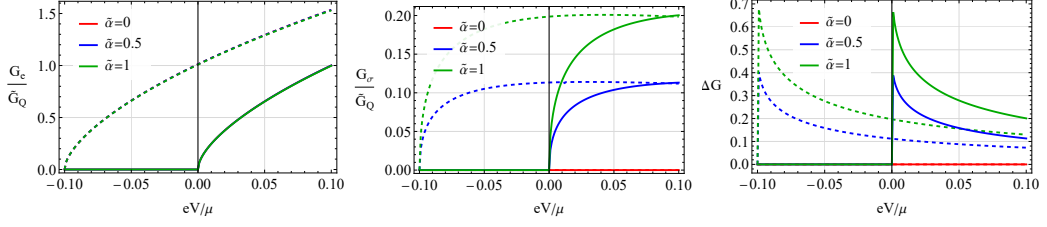


FIG. 4: The electric G_e (panel (a)) and spin G_σ (panel (b)) conductances as well as the conductance asymmetry ΔG (panel (c)). Solid and dashed lines correspond to $\tilde{J} = 1$ and $\tilde{J} = 0.9$, respectively. The spin-splitting vector $\tilde{\alpha}$ is perpendicular to the interface, $\tilde{\alpha}_y = 0$. We use Eqs. (37), (38), and (39). In all panels, we set $Z = 0$.

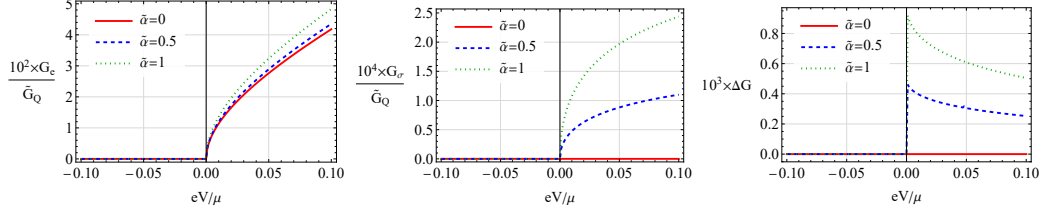


FIG. 5: The electric G_e (panel (a)) and spin G_σ (panel (b)) conductances as well as the conductance asymmetry ΔG (panel (c)). The spin-splitting vector $\tilde{\alpha}$ is perpendicular to the interface, $\tilde{\alpha}_y = 0$. We use Eqs. (37), (38), and (39). In all panels, we set $\tilde{J} = 1$ and $Z = 10$.

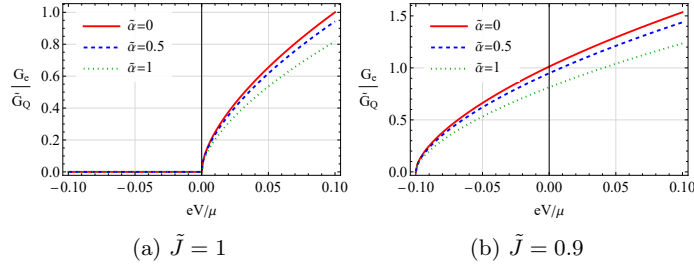


FIG. 6: The electric G_e conductance for $\tilde{J} = 1$ (panel (a)) and $\tilde{J} = 0.9$ (panel (b)). The spin-splitting vector $\tilde{\alpha}$ is parallel to the interface, $\tilde{\alpha}_x = 0$. We use Eq. (37) and set $Z = 0$.

The results for the spin-splitting vector normal to the interface, i.e., $\tilde{\alpha}_x = 0$, are shown in Fig. 6. The spin conductance vanishes, and there is no spin-filtering in this case. Unlike the case $\tilde{\alpha}_y = 0$, the electric conductance is more sensitive to the spin-splitting vector, cf. Figs. 4 and 6.

The absence of spin-filtering when the spin-splitting vector is parallel to the interface follows from a symmetry argument: the planar interface does not break the symmetry of the Fermi surface and the spin polarization $\varepsilon_{k_y, s} \leftrightarrow \varepsilon_{-k_y, -s}$. Then, the probability of tunneling from the metal into the parts of the Fermi surface in the p -wave magnet with a different spin polarization is the same, and, as a result, the conductance is insensitive to the spin of impinging particles. On the other hand, $\varepsilon_{k_x, s} \leftrightarrow \varepsilon_{-k_x, -s}$ is no longer a symmetry of the system. Therefore, we may expect different probabilities of tunneling for spin-up and spin-down electrons, as is confirmed by the results in Figs. 4 and 5.

IV. NONLINEAR TRANSPORT

In this section, we calculate the electric and spin transport properties of bulk p -wave magnets. We use the semiclassical approach where the distribution function satisfies the following kinetic equation:

$$-e\mathbf{E} \cdot \partial_{\mathbf{k}} f = -\frac{f}{\tau} \quad (41)$$

Here, $f_{eq} = 1/[e^{(\varepsilon_{\mathbf{k}} - \mu)/T} + 1]$ is the equilibrium distribution function and τ is the relaxation time. In writing Eq. (41), we assume a uniform and time-independent electric field \mathbf{E} . For simplicity, we focus on the case with a single filled band without any inter-sectoral coupling; in the effective model given in Eq. (2) in the main text, we set $|\mu| < |J|$. This allows us to neglect the inter-band scattering and use the simplest form of the collision integral for inelastic scattering in the relaxation-time approximation; the results will also hold if elastic scattering is added.

We solve Eq. (41) perturbatively in E :

$$f = f_{eq} + f^{(1)} + f^{(2)} + \dots, \quad (42)$$

where

$$f^{(1)} = e\tau (\mathbf{E} \cdot \partial_{\mathbf{k}}) f_{eq}, \quad (43)$$

$$f^{(2)} = e\tau (\mathbf{E} \cdot \partial_{\mathbf{k}}) f^{(1)} = e^2\tau^2 (\mathbf{E} \cdot \partial_{\mathbf{k}}) (\mathbf{E} \cdot \partial_{\mathbf{k}}) f_{eq}. \quad (44)$$

A. First-order response

The first-order contribution to the electric current density is defined as

$$\mathbf{j}_{el}^{(1)} = -e \int \frac{d\mathbf{k}}{(2\pi)^2} \mathbf{v} f^{(1)} = -e^2\tau \int \frac{d\mathbf{k}}{(2\pi)^2} \mathbf{v} (\mathbf{E} \cdot \partial_{\mathbf{k}}) f_{eq}, \quad (45)$$

where $\mathbf{v} = \partial_{\mathbf{k}}\varepsilon_{\mathbf{k}}$ is the group velocity. We consider zero-temperature limit $T \rightarrow 0$ and replace $\partial_{\mathbf{k}} \rightarrow \mathbf{v}\partial_{\varepsilon}$. Then,

$$\mathbf{j}_{el}^{(1)} = e^2\tau \int \frac{d\mathbf{k}}{(2\pi)^2} \mathbf{v} (\mathbf{E} \cdot \mathbf{v}) \delta(\varepsilon_{\mathbf{k}} - \mu). \quad (46)$$

In the case of the spin current density, we take into account the spin texture of the Fermi surface and replace the group velocity with the mean value of the spin current operator:

$$\langle \hat{\mathbf{j}}_{\sigma} \rangle = \psi^{\dagger} \hat{\mathbf{j}}_{\sigma} \psi, \quad (47)$$

where ψ is the eigenfunction of the effective Hamiltonian. Then,

$$\mathbf{j}_{\sigma}^{(1)} = e^2\tau \int \frac{d\mathbf{k}}{(2\pi)^2} \langle \hat{\mathbf{j}}_{\sigma} \rangle (\mathbf{E} \cdot \mathbf{v}) \delta(\varepsilon_{\mathbf{k}} - \mu). \quad (48)$$

For our model with the low-energy Hamiltonian (10), the energy spectrum is

$$\tilde{\varepsilon}_{\tilde{\mathbf{k}},\pm} = \tilde{k}^2 \pm \sqrt{\tilde{J}^2 + (\tilde{\boldsymbol{\alpha}} \cdot \tilde{\mathbf{k}})^2}, \quad (49)$$

where we used dimensionless variables. The spectrum is doubly degenerate in the sectoral degree of freedom η . We assume $\tilde{J} > 1$: in this case, only the lower band $\tilde{\varepsilon}_{\tilde{\mathbf{k}},-}$ is filled, the upper band $\tilde{\varepsilon}_{\tilde{\mathbf{k}},+}$ is empty and can be disregarded in the DC transport.

The group velocity for the lower band reads

$$\tilde{\mathbf{v}} = \left(\tilde{\mathbf{k}} + \frac{\tilde{\boldsymbol{\alpha}}}{2} S_{z,-} \right). \quad (50)$$

Here, $\tilde{v} = mv/k_F$ and

$$S_{z,\pm} = \psi^{\dagger} \sigma_z \psi = \pm \frac{(\tilde{\boldsymbol{\alpha}} \cdot \tilde{\mathbf{k}})}{\sqrt{\tilde{J}^2 + (\tilde{\boldsymbol{\alpha}} \cdot \tilde{\mathbf{k}})^2}} \quad (51)$$

is the spin polarization per sector.

To determine the mean value of the spin current (47), we use the eigenfunction ψ_{η} in Eq. (31) and the following spin current operator:

$$\hat{\mathbf{j}}_{\sigma} = \frac{i\mathbf{k}}{m} \sigma_z + \boldsymbol{\alpha}. \quad (52)$$

The result reads

$$\langle \hat{\mathbf{j}}_\sigma \rangle = \frac{k_F}{m} \left(\tilde{\mathbf{k}} S_{z,-} + \frac{\tilde{\boldsymbol{\alpha}}}{2} \right). \quad (53)$$

As follows from Eqs. (46) and (48), where Eqs. (50) and (53) were used, the electric and spin conductivities are

$$\begin{aligned} \sigma_{ij}^{(el)} &= 2\sigma_0 \sum_{\eta=\pm} \int_0^\infty \tilde{k} d\tilde{k} \int_0^{2\pi} d\theta \left(\tilde{k}_i + \frac{\tilde{\alpha}_i}{2} S_z \right) \left[\tilde{k}_j - \frac{\tilde{\alpha}_j}{2} \frac{(\tilde{\boldsymbol{\alpha}} \cdot \tilde{\mathbf{k}})}{\sqrt{\tilde{J}^2 + (\tilde{\boldsymbol{\alpha}} \cdot \tilde{\mathbf{k}})^2}} \right] \\ &\times \frac{\delta((\tilde{k} - \tilde{k}_+)(\tilde{k} - \tilde{k}_-))}{|\partial_{\tilde{k}} \tilde{\varepsilon}_-|} \end{aligned} \quad (54)$$

and

$$\begin{aligned} \sigma_{ij}^{(\sigma)} &= 2\sigma_0 \sum_{\eta=\pm} \int_0^\infty \tilde{k} d\tilde{k} \int_0^{2\pi} d\theta \left(\tilde{k}_i S_z + \frac{\tilde{\alpha}_i}{2} \right) \left[\tilde{k}_j - \frac{\tilde{\alpha}_j}{2} \frac{(\tilde{\boldsymbol{\alpha}} \cdot \tilde{\mathbf{k}})}{\sqrt{\tilde{J}^2 + (\tilde{\boldsymbol{\alpha}} \cdot \tilde{\mathbf{k}})^2}} \right] \\ &\times \frac{\delta((\tilde{k} - \tilde{k}_+)(\tilde{k} - \tilde{k}_-))}{|\partial_{\tilde{k}} \tilde{\varepsilon}_-|}, \end{aligned} \quad (55)$$

respectively. Here, $\sigma_0 = e^2 \tau \mu / \pi$ is the conductivity of a metal (i.e., at $\tilde{J} = 0$ and $\tilde{\alpha} = 0$).

For the sake of definiteness, we direct the x -axis along the spin-splitting vector $\tilde{\boldsymbol{\alpha}}$, $(\tilde{\boldsymbol{\alpha}} \cdot \tilde{\mathbf{k}}) = \tilde{\alpha} \tilde{k} \cos \theta$. Then,

$$\tilde{k}_\pm = \sqrt{1 + \frac{\tilde{\alpha}^2 \cos^2 \theta}{2} \pm \sqrt{\tilde{J}^2 - 1 + \left(1 + \frac{\tilde{\alpha}^2 \cos^2 \theta}{2}\right)^2}}. \quad (56)$$

Assuming $\tilde{\alpha} \ll 1$, integrating over \tilde{k} , and expanding up to the second order in $\tilde{\alpha}$, we obtain

$$\sigma_{xx}^{(el)} \approx \sigma_0 \sum_{\eta=\pm} \int_0^{2\pi} d\theta (1 + |\tilde{J}|) \cos^2 \theta \left(1 - \tilde{\alpha}^2 \frac{5 - 3 \cos(2\theta)}{8|\tilde{J}|} \right) = \sigma_0 (1 + |\tilde{J}|) \left(1 - \frac{7\tilde{\alpha}^2}{16\tilde{J}} \right) \quad (57)$$

and

$$\sigma_{yy}^{(el)} \approx \sigma_0 \sum_{\eta=\pm} \int_0^{2\pi} d\theta (1 + |\tilde{J}|) \sin^2 \theta \left(1 + \tilde{\alpha}^2 \frac{3 \cos^2 \theta}{4|\tilde{J}|} \right) = \sigma_0 (1 + |\tilde{J}|) \left(1 + \frac{3\tilde{\alpha}^2}{16|\tilde{J}|} \right). \quad (58)$$

The Hall conductivity $\sigma_{xy}^{(el)}$ and the spin conductivity tensor $\sigma_{ij}^{(\sigma)}$ vanish after the angular integration.

We show the conductivity (54) together with the asymptotes (57) and (58) in Fig. 7. The decrease of the conductivity along the direction of $\tilde{\boldsymbol{\alpha}}$ can be understood from the band structure: with the rise of $\tilde{\alpha}$, the energy dispersion becomes more shallow along $\tilde{\boldsymbol{\alpha}}$ leading to the decrease of the group velocity; the trend is opposite in the direction perpendicular to $\tilde{\boldsymbol{\alpha}}$.

B. Second-order response

The second-order contribution to the electric current density is defined as

$$\mathbf{j}^{(2)} = -e \int \frac{d\mathbf{k}}{(2\pi)^2} \mathbf{v} f^{(2)} = -e^3 \tau^2 \int \frac{d\mathbf{k}}{(2\pi)^2} \mathbf{v} (\mathbf{E} \cdot \partial_{\mathbf{k}}) (\mathbf{E} \cdot \partial_{\mathbf{k}}) f_{eq}, \quad (59)$$

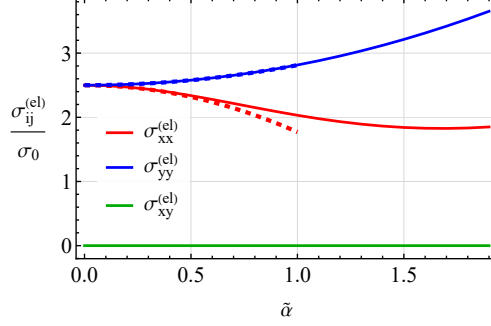


FIG. 7: The electric conductivity tensor as a function of the spin-splitting vector $\tilde{\alpha}$. We use Eq. (54) for exact results (solid lines) and Eqs. (57) and (58) for the approximate results (dashed lines). The spin conductivity tensor vanishes $\sigma_{ij}^{(\sigma)} = 0$. We set $\tilde{J} = 1.5$.

where $\langle f^{(2)} \rangle_{\varepsilon}$ does not contribute to the current. We find it convenient to separate two contributions in Eq. (59):

$$\mathbf{j}^{(2,1)} = e^3 \tau^2 \int \frac{d\mathbf{k}}{(2\pi)^2} \mathbf{v} \delta(\varepsilon_{\mathbf{k}} - \mu) (\mathbf{E} \cdot \partial_{\mathbf{k}}) (\mathbf{E} \cdot \mathbf{v}), \quad (60)$$

$$\mathbf{j}^{(2,2)} = e^3 \tau^2 \int \frac{d\mathbf{k}}{(2\pi)^2} \mathbf{v} (\mathbf{E} \cdot \mathbf{v}) (\mathbf{E} \cdot \partial_{\mathbf{k}}) \delta(\varepsilon_{\mathbf{k}} - \mu). \quad (61)$$

The derivative from the δ -function can be tackled by using the following formula:

$$\begin{aligned} \int d\mathbf{k} F(\mathbf{k}) \partial_{k_i} \delta(\varepsilon_{\mathbf{k}} - \mu) &= \int d\varepsilon \int d\theta J(\varepsilon, \theta) v_i F(\varepsilon, \theta) \partial_{\varepsilon} \delta(\varepsilon - \mu) \\ &= - \int d\varepsilon \int d\theta \delta(\varepsilon - \mu) \partial_{\varepsilon} [J(\varepsilon, \theta) v_i F(\varepsilon, \theta)] = - \int d\mathbf{k} \delta(\varepsilon - \mu) \frac{1}{J(\varepsilon, \theta)} \partial_{\varepsilon} [J(\varepsilon, \theta) v_i F(\varepsilon, \theta)], \end{aligned} \quad (62)$$

where $F(\mathbf{k})$ is a differentiable function of momentum, $J(\varepsilon, \theta) \equiv J(\mathbf{k}) = \tilde{k} \left| \frac{\partial \tilde{k}}{\partial \tilde{\varepsilon}} \right|$ is the Jacobian, and we integrated by parts in the second line.

Therefore, we have

$$\mathbf{j}^{(2,2)} = - \frac{e^3 \tau^2}{(2\pi)^2} \int d\mathbf{k} \delta(\varepsilon_{\mathbf{k}} - \mu) \frac{1}{J(\mathbf{k})} \partial_{\varepsilon} [J(\mathbf{k}) \mathbf{v} (\mathbf{E} \cdot \mathbf{v}) (\mathbf{E} \cdot \mathbf{v})]. \quad (63)$$

For the spin current, we replace the first group velocity \mathbf{v} in Eqs. (60) and (61) with the mean value of the spin current, see Eq. (47).

The electric response tensor $\chi_{ijl}^{(el)}$ defined as $j_{el,i}^{(2)} = \chi_{ijl}^{(el)} E_j E_l$ is

$$\chi_{ijl}^{(el)} = \chi_0 \sum_{\eta=\pm} \int_0^{\infty} \tilde{k} d\tilde{k} \int_0^{2\pi} \frac{d\theta}{2\pi} \delta(\tilde{\varepsilon} - 1) \left[\tilde{v}_i \partial_{\tilde{k}_j} \tilde{v}_l - \frac{2}{J(\tilde{k}, \theta)} \partial_{\tilde{\varepsilon}} \left\{ J(\tilde{k}, \theta) \tilde{v}_i \tilde{v}_j \tilde{v}_l \right\} \right], \quad (64)$$

where $\chi_0 = e^3 \tau^2 k_F / m$ and we also included the summation over the two sectors; it leads to an overall factor of 2. As required by the time-reversal symmetry, the response tensor $\chi_{ijl}^{(el)}$ vanishes.

For the spin response tensor $\chi_{ijl}^{(\sigma)}$ defined as $j_{\sigma,i}^{(2)} = \chi_{ijl}^{(\sigma)} E_j E_l$, components $\chi_{ijl}^{(\sigma,1)}$ and $\chi_{ijl}^{(\sigma,2)}$, we have

$$\chi_{ijl}^{(\sigma)} = \chi_0 \sum_{\eta=\pm} \int_0^{\infty} \tilde{k} d\tilde{k} \int_0^{2\pi} \frac{d\theta}{2\pi} \delta(\tilde{\varepsilon} - 1) \left\{ \left(\tilde{k}_i + \frac{\tilde{\alpha}_i}{2} S_z \right) \partial_{\tilde{k}_j} \tilde{v}_l - \frac{2}{J(\tilde{k}, \theta)} \partial_{\tilde{\varepsilon}} \left[J(\tilde{k}, \theta) \left(\tilde{k}_i + \frac{\tilde{\alpha}_i}{2} S_z \right) \tilde{v}_j \tilde{v}_l \right] \right\}. \quad (65)$$

We use Eq. (65) in Fig. 4 in the main text.

[1] L. S. Levitov and A. V. Shytov, *Green's functions. Theory and practice* (FizMatLit-Nauka, Moscow, 2003).

- [2] G. D. Mahan, *Many-Particle Physics* (Springer New York, New York, 2000) p. 785.
- [3] G. E. Blonder, M. Tinkham, and T. M. Klapwijk, Transition from metallic to tunneling regimes in superconducting microconstrictions: Excess current, charge imbalance, and supercurrent conversion, *Phys. Rev. B* **25**, 4515 (1982).